Third harmonic upconversion enhancement from a single semiconductor nanoparticle coupled to a plasmonic antenna

Heykel Aouani[1†*], Mohsen Rahmani[1†], Miguel Navarro-Cía[2] and Stefan A. Maier[1]

[1] The Blackett Laboratory, Department of Physics, Imperial College London, London SW7 2AZ, United Kingdom,

[2] Optical and Semiconductor Devices Group, Department of Electrical and Electronic Engineering, Imperial College London, London SW7 2BT, United Kingdom,

[†] These authors contributed equally to this work

[*]e-mail: h.aouani@imperial.ac.uk

The ability to convert low energy quanta into a quantum of higher energy is of great interest for a variety of applications such as bioimaging[1], drug delivery[2] and photovoltaics[3]. Although high nonlinear conversion efficiency can be achieved using macroscopic nonlinear crystals, upconverting light at the nanometer scale remains challenging because the subwavelength scale of materials prevents exploiting phase matching processeses[4]. Light-plasmon interactions occurring in noble metal nanostructures have offered alternative opportunities for nonlinear upconversion of infrared light, but conversion efficiency rates remain extremely low due the weak penetration of the exciting fields into the metal[5]. Here we show that the third harmonic generation (THG) from an individual semiconductor indium tin oxide (ITO) nanoparticle is significantly enhanced when coupled within a plasmonic gold dimer. The plasmonic dimer acts as a receiving optical antenna[6], confining the incident far field radiation into a near field localized at its gap. Meanwhile, the ITO nanoparticle located at the plasmonic dimer gap acts as a localized nonlinear transmitter upconverting three incident photons at frequency ω into a photon at frequency 3ω. This hybrid nanodevice provides third harmonic generation enhancements of up to 10^6 folds compared to an isolated ITO nanoparticle, with an effective third order susceptibility up to 3.5×10^3 nm^2/V^2 and conversion efficiency of 0.0007%. We also show that the upconverted third

harmonic emission can be exploited to probe the near-field intensity at the plasmonic dimer gap.

Efficiently converting multiple low energy photons into a photon of higher energy is of great interest in many areas of science and technology. At macroscopic scales, coherent conversion processes are intensively exploited for upconverting tunable laser light[7] and for fast label-free imaging of biological samples[8]. At nanoscopic scales, luminescence upconversion subwavelength crystals can play the role of carriers for intracellular drug delivery[9] and are considered as promising candidates to overcome the Shockley-Queisser efficiency limit of single-junction solar cells[3,10]. Technological advances realized in nanoengineering of noble metals have offered new opportunities for nonlinearly upconverting infrared pulsed light within nanometric volumes *via* the exploitation of coherent harmonic generation processes from plasmonic structures excited at resonance[5]. While most of seminal works have focused on the nonlinear intrinsic responses from plasmonic structures[11-13], only few recent studies have investigated so far the enhanced nonlinear extrinsic responses provided by plasmonic couplings[4]. Such configurations are particularly suitable for electrical[14] and optical[15] control of nonlinear properties from bulk materials adjacent to plasmonic structures, or for plasmon-enhanced generation of coherent extreme-ultraviolet light from gas jets[16]. Despite significant advances, achieving high harmonic conversion efficiencies of light from nonlinear nanostructured materials remains a challenge to address.

In this letter, we introduce and experimentally demonstrate the viability of a novel subwavelength harmonic conversion system made of a single indium tin oxide nanoparticle decorated with a plasmonic dimer (Fig. 1a). Although the THG from an isolated ITO nanoparticle is relatively weak, localized plasmonic coupling dramatically enhances by several orders of magnitude its three-photon upconversion, which enables to unambiguously discriminate the third harmonic signal from the ITO nanoparticle from the strong intrinsic nonlinear metallic background[17-19]. Due to the non-absorbing nature of the nonlinear generation processes, the third harmonic scattering from the ITO nanoparticle is mainly sensitive to the local intensity excitation in the plasmonic gap region, thus enabling an

accurate probing of near-field intensities with a far-field method.

The nonlinear upconversion nanosystems were realized *via* two-steps electron-beam lithography and a combination of etch-down and lift-off methods, with a well-controlled spatial alignment. Single 25 nm diameter ITO nanoparticles were generated by ion beam etching followed by a lift-off procedure for creating well aligned gold dimer decorations (Fig. 1b). This led to the completion of the nonlinear upconversion system made of an ITO nanoparticle at the gap of a plasmonic dimer presented in Fig. 1b,c. Due to the non-directional deposition nature of the ITO sputtering process, the combination of etch-down and lift-off methods is essential to realize the hybrid nanostructures presented in this work, hence the differences in the fabrication approach compared to those recently used for subwavelength plasmonic mapping[20,21] and probing[22] investigations, or for controlling the optical responses of plasmonic antennas by nanomaterial loading[23].

Finite-difference time-domain (FDTD) simulations exploiting the total-field scattered-field formulation were performed to provide the spatial distribution of the intensity enhancement and extinction spectrum of the fabricated dimers (Fig. 1d,e). The dimer models are generated from the SEM pictures such as the one presented in Fig. 1c, whereas the ITO nanoparticles are considered ideal 25 nm diameter cylinders localized at the position determined from the SEM pictures. The optical dielectric functions of Au, Cr (adhesion layer), SiO_2 (substrate) and ITO are fitted to experimental data[24,25]. As highlighted in previous works[26], the introduction of a dielectric nanoparticle at the gap of a metallic optical antenna dimer leads to a spectral red-shift of its plasmonic resonance (Fig. 1e).

The linear experimental characterization of the fabricated structures in array configuration (112 nanostructures per array, pitch of 2 μm) was performed using a commercial Fourier transform infrared spectroscopy (FTIR) apparatus, (see Supplementary Section S2 for more information). The corresponding extinction spectra (defined as 1-transmission) for the 35 nm nanorod dimer with and without an ITO nanoparticle at its gap is presented in Fig. 1f. A slight red-shift of the resonance peak position is observed for both configurations compared to the numerical predictions of Fig. 1e, which can be attributed to minor defects related to the

fabrication process (thickness of the gold layer, roughness...), but the shapes of the measured extinction cross sections agree well with the simulated spectra. From Fig. 1f, one can also observe that the fundamental excitation wavelength set for the nonlinear investigations matches with the plasmonic resonance of the nanorod dimer not coupled to an ITO nanoparticle.

We started our nonlinear experimental investigations by measuring the THG from an isolated ITO nanoparticle (see Supplementary Section S3 for more information). Under excitation at frequency ω, the third order ITO susceptibility[25] $\chi^{3\omega}$= 3.36 nm^2/V^2 induces a nonlinear polarization $\boldsymbol{P}^{3\omega}= \varepsilon_0\chi^{3\omega}\boldsymbol{E}^{\omega}\boldsymbol{E}^{\omega}\boldsymbol{E}^{\omega}$, which in turns generates a radiation of intensity $I^{3\omega} \alpha |\boldsymbol{P}^{3\omega}|^2$. As expected, a fundamental femtosecond excitation at λ= 1500 nm gives rise to the instantaneous third harmonic ITO response centred at λ= 500 nm presented in Fig. 2a. From this spectrum, the THG radiated power is estimated to be 1.94×10^{-20} W, corresponding to an upconversion efficiency of 5.8×10^{-10} %. This weak efficiency is dramatically enhanced when the single ITO nanoparticle is decorated with a 35 nm gap nanorod plasmonic dimer (Fig. 2b) under parallel polarized excitation. The third harmonic peak intensity generated by the hybrid upconversion system is increased by 6 orders of magnitude compared to an isolated ITO nanoparticle, leading to a third harmonic power of 2.17×10^{-14} W and an upconversion efficiency of 7×10^{-4} %. Notice that unlike the linear characterization performed by FTIR spectroscopy, all nonlinear measurements with hybrid nanostructures have been conducted on single entities. Such huge increase of the nonlinear signal essentially results from the high excitation intensity enhancement created by plasmonic coupling[27], but can also be viewed as an improvement of the third order ITO susceptibility $\chi^{3\omega}$ (see Supplementary Section S6 for more discussions). Exploiting the experimental data, we compute a third order effective susceptibility of 3543 nm^2/V^2 for the 25 nm ITO nanoparticle decorated with the plasmonic dimer, which is a susceptibility 7 order of magnitude higher than those reported with nonlinear macroscopic crystals[28].

As non-negligible intrinsic third harmonic responses from plasmonic antennas were recently reported[17-19], careful attention has been devoted to quantify the intrinsic third harmonic background from the plasmonic dimers by conducting extensive sets of multi-wavelength measurements (data available in Supplementary Section S4) and nonlinear FDTD simulations for the limiting cases with either $\chi_{Au}^{(3)}$ or $\chi_{ITO}^{(3)}$ set to zero (data available in Supplementary Section S8). These results combined with a gap size dependence analysis and an extensive set of multi-wavelength measurements indicate that THG from the ITO nanoparticle coupled to the plasmonic dimer is 16 times higher (THG upconversion efficiency 3 orders of magnitude higher, data provided in Supplementary Section S4) than the THG background from the metallic dimer itself, thus confirming that the nonlinear signal mainly originates from ITO[29].

The nonlinear phenomenon responsible for the upconversion process requires the instantaneous capture of three infrared photons to generate a green photon, hence a cubic dependence of the radiated third harmonic with excitation intensity is expected. This trend is corroborated by the experimental measurements presented in Fig. 2c, which show that the THG intensity from the upconversion hybrid system is sensitive to the third power of the fundamental incident light. Unlike luminescent nanocrystals[3], the upconverted light from the hybrid nanosystem does not exhibit any saturation limitation, and, on the contrary, increasing the fundamental incident power leads to improving the conversion efficiency. This observation is a direct consequence of the scattering nature of harmonic generation mechanisms as opposed to the absorption nature of luminescence processes. The current limitation regarding the nonlinear upconversion efficiency is related to the laser damage threshold of the hybrid nanosystems, which prevents achieving third harmonic conversion efficiency greater than 7×10^{-4} % (more discussion available in Supplementary Section S7).

As an immediate application of high relevance for nanophotonics, we accurately quantify the excitation intensity enhancement η for various nanodimers (Fig. 3a), when their gaps are coupled to single emitters, by using an ITO nanoparticle as a probe of the near-field plasmonic intensity. From the numerical simulations shown in Fig. 3b, one can observe that any increase of the dimers' gaps leads to a reduction of plasmonic intensity enhancements,

and therefore to weaker third harmonic responses from the ITO nanoparticle. Such expectations are corroborated by the third harmonic spectral measurements displayed in Fig. 3c,e, where the THG intensity drastically decreases with increasing gap dimensions. Exploiting these data, the intensity enhancement factor η can be computed as the cube root of the ratio between the third harmonic power from the ITO nanoparticle with and without the plasmonic antenna investigated. This is further discussed in the Supplementary Section S5. The experimental values determined for η are presented in Fig. 3d,f together with numerical predictions. Excellent agreement was found between the experimental observations and the simulated data for all the probed designs. As expected from the third harmonic spectra of Fig. 2b and Fig. 3c,e, the highest intensity enhancements are provided by the 35 nm gap nanorod and 30 nm gap nanocylinder dimers, with experimental values for η of 103.6 and 49.4 respectively, and numerical predictions of 119.5 and 55.1, respectively. Lower enhancement factors were measured for the 55 nm gap nanorod and 40 nm gap nanocylinder dimers due to weaker electromagnetic couplings for increasing gaps. These excellent agreements between experimental and numerical intensity enhancements demonstrate that single nonlinear nanoparticles can play the role of subwavelength near-field probes.

In summary, we have introduced and experimentally highlighted the viability of a novel nanoscale upconversion system based on a single nonlinear nanometric particle decorated with a plasmonic motif. This nanosystem provides nonlinear upconversion enhancements up to 10^6 fold compared to an isolated ITO nanoparticle, and enable to unambiguously discriminate the nonlinear signal emitted by the ITO nanoparticle from the intrinsic nonlinear metallic background. While the plasmonic antennas presented here exhibit narrow-band resonances, tunable third harmonic upconversion nanosystems could be realized by implementing a nonlinear nanomaterial at the gap of broadband plasmonic antenna designs[30]. Finally, we demonstrated that a nonlinear nanoparticle can be used as a near-field nanoprobe to quantify the hot spot intensities in plasmonic dimers when single emitters are placed at their gaps, thus introducing a new form of nonlinear enhanced light-matter interactions at the

nanoscale and bridging the gap between the theoretical predictions of field enhancement and experimental electromagnetic nanometrology.

Methods

Sample fabrication. The third harmonic upconversion nanosystems composed of an ITO nanoparticle decorated with a plasmonic dimer were realized via combination of electron-beam lithography with etch-down and lift-off approaches, accompanied by precise alignments. Indeed, a pure lift-off approach prevents achieving nanometric size particles with dimensions smaller than 30 nm diameter via sputtering because of its non-directional deposition nature. Therefore, a quartz substrate was first covered with a 40 nm ITO film by sputtering. Hereafter, high resolution circular nanodots and alignment markers were defined in hydrogen silsesquioxane resist on the substrate by electron-beam lithography. Ion beam etching (argon ions) of the ITO layer was then performed to generate single 25 nm diameter nanoparticles, as presented in Fig 1b. Then, the sample was coated with polymethylmethacrylate and rod/ cylinder nanodimer shapes centred on a single ITO nanoparticle were defined in the resist, followed by a thermal evaporation of 2 nm chromium adhesion layer and 40 nm gold. A final lift-off step led to the completion of the upconversion system made of an ITO nanoparticle trapped in the gap of a plasmonic dimer, as presented in Fig. 1b,c. More details about sample fabrication are available in Supplementary Section S1.

Numerical simulations. We performed 3D FDTD simulations using the commercial software FDTD solution v8.6 (Lumerical Inc. Vancouver, Canada). The SEM pictures of the dimers were imported into the software to generate the dimer model according to the fabricated dimensions. The ITO nanoparticles, meanwhile, were considered as ideal Ø25nm cylinders placed at the position according to the SEM pictures. The optical dielectric functions of the different materials are taken from tabulated data: Au, Cr, SiO2 and ITO[24,25]. The dielectric dispersion of the materials was fitted in the spectral range from 1000 nm to 2000 nm by a 6-coefficient model, allowing a tolerance of 0.1 and enforcing passivity.

All simulation boundaries were set as perfect matched layers (PML) to replicate a single dimer over a semi-infinite substrate scenario. The solver-defined total-field scattered-field (TFSF) source was used to reduce computation effort since it allows defining the plane-wave excitation within the volume

enclosing only the dimer. For the linear simulations shown, the TFSF box had a size 800 nm × 500 nm × 80 nm. The *x*-polarized plane-wave excitation was incident normal to the dimer from the semi-infinite free-space, i.e., propagating along -*z*. The incident temporal pulse had spectral components ranging from 1000 nm to 2000 nm (i.e. central wavelength 1500 nm, and bandwidth of 1000 nm), and thus, its pulse length is ~6.64 fs. A conformal non-uniform mesh was used to map accurately the details of the model. The TFSF volume default grid was 7 nm × 7 nm × 2 nm. For the dimer region, the volume with dimensions 650 nm × 340 nm × 50 nm was discretized with a cubic grid of 4 nm × 4 nm × 2 nm. An even smaller cubic grid of 0.5 nm × 0.5 nm × 2 nm was overridden in the region enclosing the ITO nanoparticle and the gaps between the ITO particle and each arm of the dimer. A finer mesh size along *z* of 0.5 nm was applied for the Cr layer. The maximum simulation time was set to 300 fs. The time stepping stability factor was set to 0.99, which corresponded to a time step of $\delta t = 0.00095$ fs. The residual energy in the simulation box volume was at least 50 dB lower than its peak value to ensure that the continuous wave information obtained by discrete Fourier transformations was valid. A standard convergence test was done to ensure negligible numerical errors originated from the PML distance, the non-uniform meshing, or the monitor sampling.

The extinction cross section was calculated by the sum of the power flowing outward through a volume enclosing the TFSF source (scattering cross section) and the net power flowing inward through a rectangular cuboid inside the TFSF volume enclosing the dimer (absorption cross section). The average intensity within the ITO nanoparticle was obtained from a 3D field monitor. To generate the intensity enhancement color maps, a 2D field profile monitor recorded the field on the *xy* middle cross section plane. More linear and nonlinear simulations are presented in Supplementary Section S8.

Experimental setup. The inverted microscope developed for this work uses a Yb:KGW femtosecond PHAROS laser system as a pump of a collinear optical parametric amplifier ORPHEUS with a LYRA wavelength extension option (Light Conversion Ltd, Lithuania, pulse duration 140 fs, repetition rate 100 kHz). For nonlinear experiments, the fundamental incident wavelength is focused on the sample plane by a 0.6 NA microscope objective, and the backward-emitted third harmonic generation at 500 nm is collected via the same objective. More information about the experimental setup is available in Supplementary Section S3.

References

1. Débarre, D. *et al*. Imaging lipid bodies in cells and tissues using third-harmonic generation microscopy. *Nat. Methods* **3**, 47–53 (2006).
2. Zhou, J., Liu, Z. & Li, F. Upconversion nanophosphors for small-animal imaging. *Chem. Soc. Rev.* **41**, 1323–1349 (2012).
3. Zou, W.Q., Visser, C., Maduro, J.A., Pshenichnikov, M.S. & Hummelen, J.C. Broadband dye-sensitized upconversion of near-infrared light. *Nature Photon.* **6**, 560–564 (2012).
4. Agio, M. & Alù, A. *Optical antennas* (Cambridge University Press, 2013).
5. Kauranen, M. & Zayats, A.V. Nonlinear plasmonics. *Nature Photon.* **6**, 737–748 (2012).
6. Novotny, L. & van Hulst, N. Antennas for light. *Nature Photon*. **5**, 83–90 (2011).
7. Franken, P.A., Hill, A.E., Peter, C.W. & Weinreich, G. Generation of optical harmonics. *Phys. Rev. Lett.* **7**, 118–119 (1961).
8. Xie, X.S., Yu, J. & Yang, W.Y. Living cells as test tubes. *Science* **312**, 228–230 (2006).
9. Tian, G. *et al*. Mn^{2}+ dopant-controlled synthesis of NaYF4:Yb/Er upconversion nanoparticles for *in vivo* imaging and drug delivery. *Adv. Mater.* **24**, 1226–1231 (2012).
10. Wang, H.-Q., Batentschuk, M., Osvet, A., Pinna, L. & Brabec, C.J. Rare-earth ion doped up-conversion materials for photovoltaic applications. *Adv. Mater*. **23**, 2675–2680 (2011).
11. Lamprecht, B., Krenn, J.R., Leitner, A. & Aussenegg, F.R. Resonant and off-resonant light-driven plasmons in metal nanoparticles studied by femtosecond-resolution third-harmonic generation. *Phys. Rev. Lett.* **83**, 4421 (1999).
12. Mühlschlegel, P., Eisler, H.-J., Martin, O.J.F., Hecht, B. & Pohl, D.W. Resonant optical antennas. *Science* **308**, 1607–1609 (2005).
13. Schuck, P.J., Fromm, D.P., Sundaramurthy, A., Kino, G.S. & Moerner, W.E. Improving the mismatch between light and nanoscale objects with gold bowtie nanoantennas. *Phys. Rev. Lett.* **94**, 017402 (2005).
14. Cai, W., Vasudev, A.P. & Brongersma, M.L. Electrically controlled nonlinear generation of light with plasmonics. *Science* **333**, 1720–1723 (2011).
15. Abb, M., Albella, P., Aizpurua, J. & Muskens, O.L. All-optical control of a single plasmonic nanoantenna–ITO hybrid. *Nano Lett.* **11**, 2457–2463 (2011).

16. Kim, S. *et al*. High-harmonic generation by resonant plasmon field enhancement. *Nature* **453**, 757–760 (2008).

17. Hanke, T. *et al*. Tailoring spatiotemporal light confinement in single plasmonic nanoantennas. *Nano Lett.* **12**, 992–996 (2012).

18. Hentschel, M., Utikal, T., Giessen, H. & Lippitz, M. Quantitative modeling of the third harmonic emission spectrum of plasmonic nanoantennas. *Nano Lett.* **12**, 3778–3782 (2012).

19. Melentiev, P.N., Afanasiev, A.E., Kuzin, A.A., Baturin, S.A. & Balykin, V.I. Giant optical nonlinearity of a single plasmonic nanostructure. *Opt. Express*. **21**, 13896–13905 (2013).

20. Koller, D.M. *et al*. Superresolution Moiré mapping of particle plasmon modes. *Phys. Rev. Lett.* **104**, 143901 (2010).

21. Dregely, D., Neubrech, F., Duan, H., Vogelgesang, R. & Giessen, H. Vibrational near-field mapping of planar and buried three-dimensional plasmonic nanostructures. *Nat. Commun.* **4**, 2237 (2013).

22. Bermúdez Ureña, E. *et al*. Excitation enhancement of a quantum dot coupled to a plasmonic antenna. *Adv. Mater.* **24**, OP314–OP320 (2012).

23. Liu, N. *et al*. Individual nanoantennas loaded with three-dimensional optical nanocircuit. *Nano Lett*. **13**, 142–147 (2013).

24. Palik, E.D. *Handbook of optical constants of solids* (Academic Press, 1985).

25. Humphrey, J.L. & Kuciauskas, D. Optical susceptibilities of supported indium tin oxide thin films. *J. Appl. Phys*. **100**, 113123 (2006).

26. Alaverdyan, Y. *et al*. Spectral tunability of a plasmonic antenna with a dielectric nanocrystal. *Opt. Express*. **19**, 18175–18181 (2011).

27. Giannini, V., Fernández-Domínguez, A.I., Heck, S.C. & Maier, S.A. Plasmonic nanoantennas: fundamentals and their use in controlling the radiative properties of nanoemitters. *Chem. Rev*. **6**, 3888–3912 (2011).

28. Ganeev, R.A., Kulagin, I.A., Ryasnyansky, A.I., Tugushev, R.I. & Usmanov, T. Characterization of nonlinear optical parameters of KDP, LiNbO3 and BBO crystals. *Opt. Commun.* **229**, 403–412 (2004).

29. Harutyunyan, H., Volpe, G., Quidant, R. & Novotny, L. Enhancing the nonlinear optical response using multifrequency gold-nanowire antennas. *Phys. Rev. Lett.* **108**, 217403 (2012).

30. Navarro-Cia, M. & Maier S.A. Broad-band near-infrared plasmonic nanoantennas for higher harmonic generation. *ACS Nano* **6**, 3537–3544 (2012).

Acknowledgments

We thank Alexandra Rakovich for the fabrication of preliminary samples, Yannick Sonnefraud for his help on sample characterization, and Vincenzo Giannini and Antonio I. Fernández-Domínguez for stimulating discussions. This work was funded by the Engineering and Physical Sciences Research Council (EPSRC) through Active Plasmonics programme, the Leverhulme Trust, the U.S. Army International Technology Centre Atlantic (USAITC-A) and the Office of Naval Research (ONR and ONR Global). M.N.-C. is supported by an Imperial College Junior Research Fellowship.

Author contributions

H.A. and S.A.M. conceived and supervised the project. M.N.-C. provided the numerical work, M.R. fabricated the samples and H.A. performed the experiments. H.A. wrote the manuscript. All authors participated to data processing, analysis, discussions and manuscript preparation.

Additional information

Supplementary information accompanies this paper at www.nature.com/naturenanotechnology. Reprints and permission information is available online at http://npg.nature.com/reprintsandpermissions/. Correspondence and requests for materials should be addressed to H.A.

Competing financial interests

The authors declare no competing financial interests.

FIGURES

Figure 1 | Nonlinear upconversion nanosystem. (**a**), Schematic of the third harmonic radiation from a single ITO nanoparticle decorated with a plasmonic nanorod dimer. For greater clarity, we represented a transmission configuration here but in our experiment we collected the backward-emitted third harmonic signal. (**b**), SEM images of an array of upconversion systems. In a first step, 25 nm dots are generated via etch-down method (left side SEM images), and in a second step the gold dimer decoration is created around by a lift-off procedure (right side SEM image). Arrows in left side SEM image indicate the position of the ITO nanoparticles. Scale bar, 1 □m. (**c**), SEM image of a single nonlinear upconversion system. Scale bar, 200 nm. (**d**), FDTD computation of the intensity enhancement along the middle cross-sectional plane for □ = 1500 nm and an incident plane-wave polarized parallel to the dimer's axis. (**e**), Simulated extinction cross section (dash-dot-dot line) of the 35 nm gap nanorod dimer with (blue) and without (purple) an ITO nanoparticle at its gap and intensity enhancement (solid line) at the centre of the ITO nanoparticle when coupled to the plasmonic dimer. (**f**), Experimental extinction cross section of the 35 nm gap nanorod dimer array with (blue) and without (purple) an ITO nanoparticle at its gap. The red rectangle indicates the spectral position of the fundamental excitation wavelength used for the nonlinear measurements.

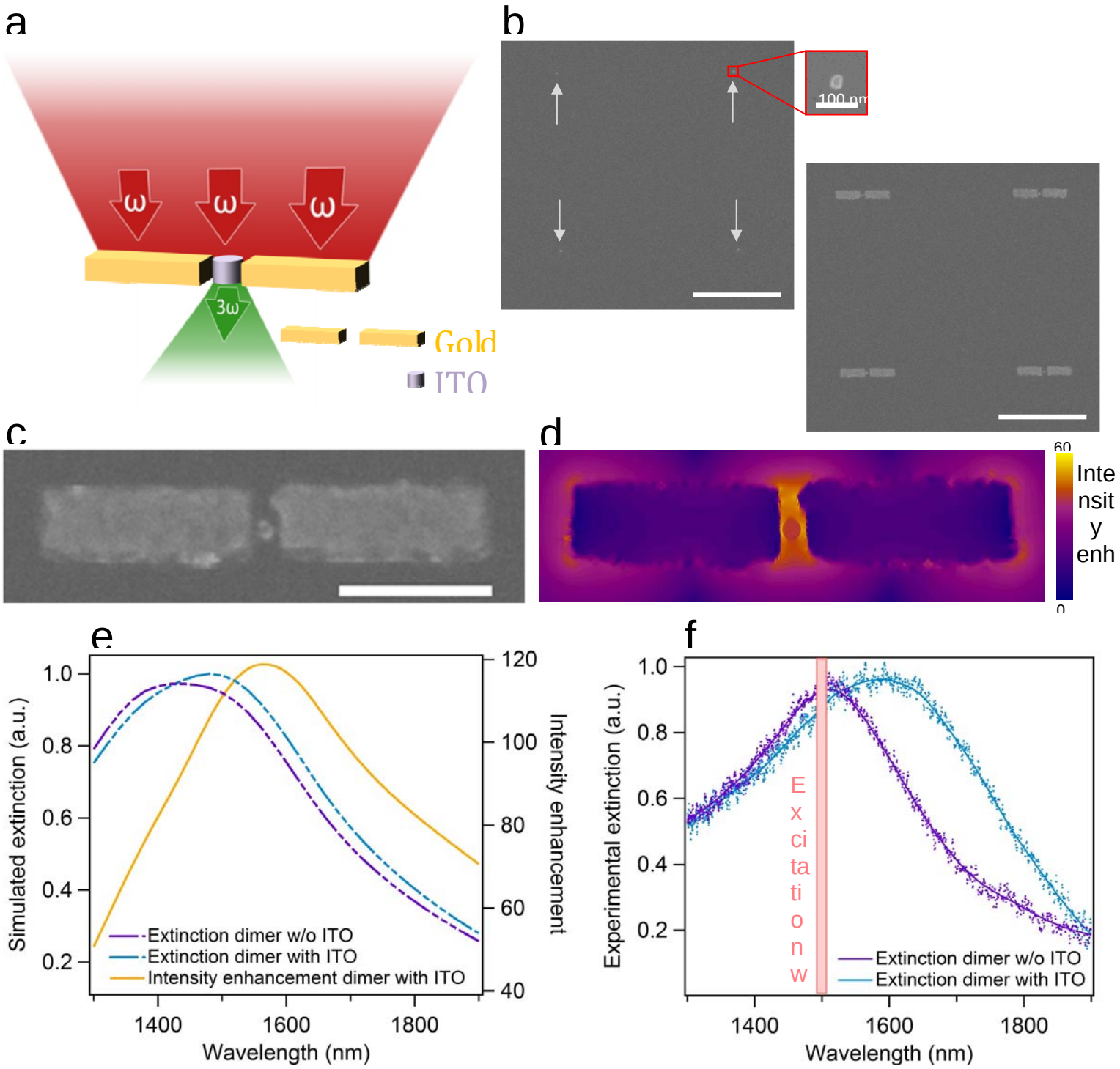

Figure 2 | Three-photon upconversion enhancement from a single ITO nanoparticle decorated with a plasmonic dimer. (**a**), Third harmonic generation spectrum of an isolated 25 nm ITO nanoparticle for an incident wavelength at 1500 nm (average incident power of 50 ?W, peak intensities of 45.7 GW/cm2). (**b**), Third harmonic generation spectrum of single ITO nanoparticle localized at the centre of a 35 nm gap nanorods dimer under parallel polarized excitation (average incident power of 50 ?W, peak intensities of 45.7 GW/cm2). (**c**), Evolution of the third harmonic intensity as a function of the fundamental incident power. The blue dots indicate the experimental data and the black line is a numerical fit with a third order power function

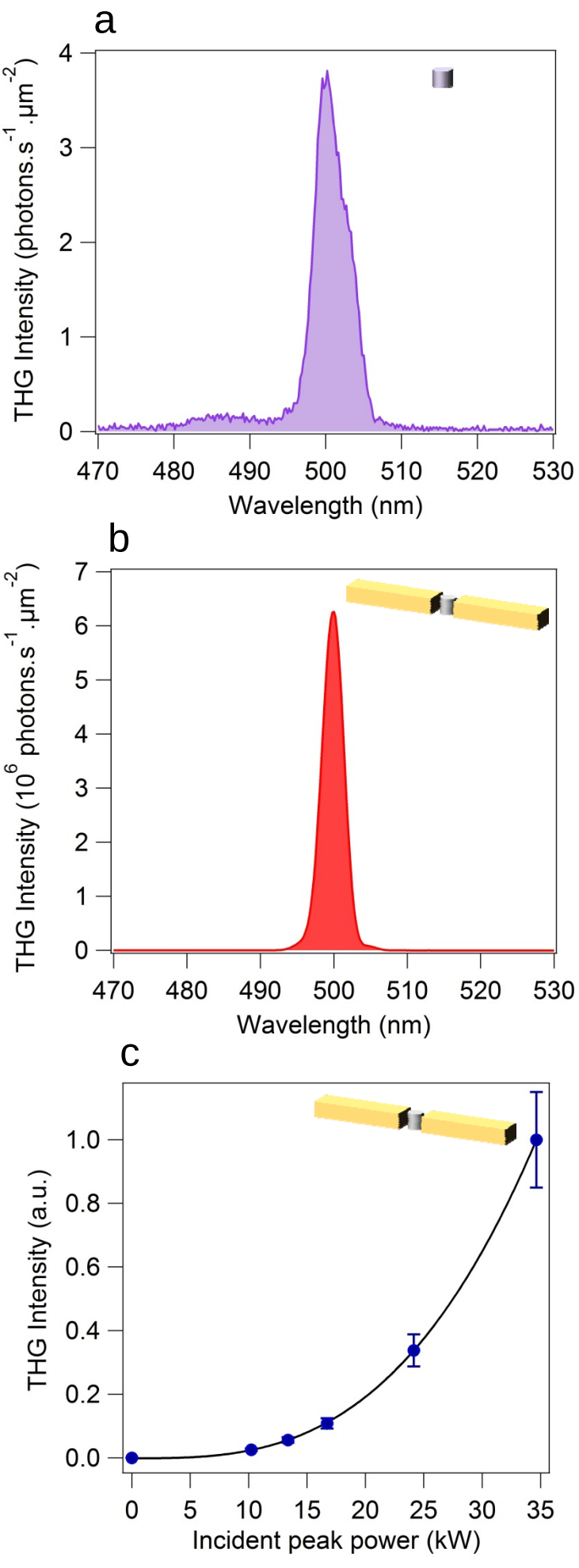

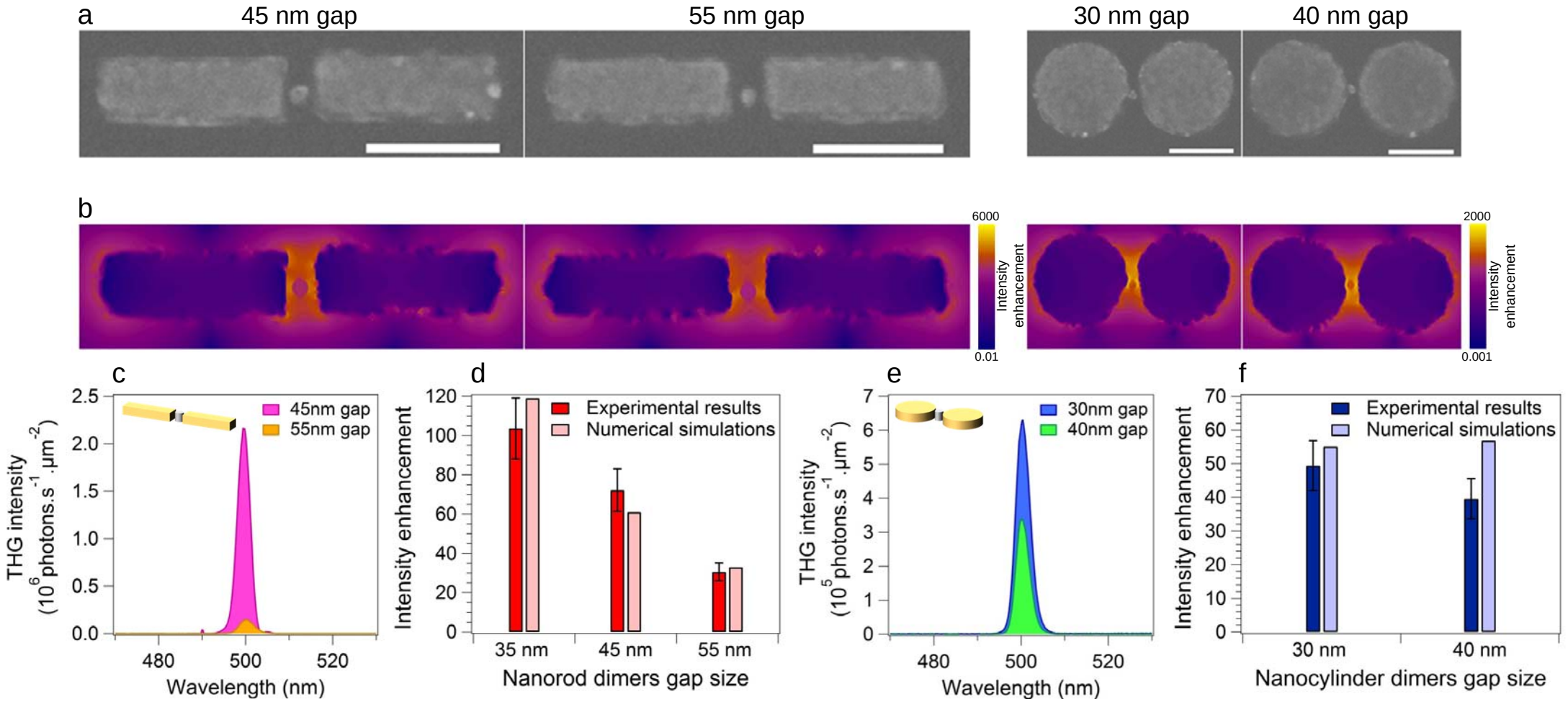
a
45 nm gap
55 nm gap
30 nm gap
40 nm gap
b
6000
Intensity enhancement
0.01
2000
Intensity enhancement
0.001
c
45nm gap
55nm gap
THG intensity (10^6 photons.s^-1.µm^-2)
Wavelength (nm)
d
Experimental results
Numerical simulations
Intensity enhancement
35 nm
45 nm
55 nm
Nanorod dimers gap size
e
30nm gap
40nm gap
THG intensity (10^5 photons.s^-1.µm^-2)
Wavelength (nm)
f
Experimental results
Numerical simulations
Intensity enhancement
30 nm
40 nm
Nanocylinder dimers gap size